

Article

Tuning HAuCl_4 /Sodium Citrate Stoichiometry to Fabricate Chitosan-Au Nanocomposites

Luis R. Torres-Ferrer ¹, José M. López-Romero ², Juan Mendez-Nonell ³, Maria J. Rivas-Arreola ⁴, Marisa Moreno-Ríos ⁵, Erika O. Ávila-Dávila ⁵, Evgeny Prokhorov ² , Yuriy Kovalenko ² , Diana G. Zárate-Triviño ^{6,*}, Javier R. Revilla-Vazquez ^{7,*} , Marco A. Meraz-Rios ^{8,*}  and Gabriel Luna-Barcenas ^{2,*} 

- ¹ Nanosciences & Nanotechnology Program, Cinvestav Zacatenco, Ciudad de Mexico 07360, Mexico; luisruben.torres@cinvestav.mx
- ² Cinvestav Querétaro, Querétaro 76230, Mexico; jm.lopez@cinvestav.mx (J.M.L.-R.); prokhorov@cinvestav.mx (E.P.); kovalenko.yuriy@gmail.com (Y.K.)
- ³ Cinvestav Saltillo, Ramos Arizpe 25900, Mexico; jmendeznonell@cinvestav.mx
- ⁴ Department of Sciences & Engineering, Universidad Iberoamericana, San Andrés Cholula 72820, Mexico; mariajose.rivas@iberopuebla.mx
- ⁵ Department of Postgraduates Studies and Investigation, Tecnológico Nacional de Mexico, Instituto Tecnológico de Pachuca, Pachuca 42080, Mexico; marisa.mr@pachuca.tecnm.mx (M.M.-R.); erika.ad@pachuca.tecnm.mx (E.O.Á.-D.)
- ⁶ Immunology and virology Laboratory, Universidad Autónoma de Nuevo León, Monterrey 64450, Mexico
- ⁷ Department of Engineering & Technology, Division of Chemical Sciences, FES-Cuautitlan, Universidad Nacional Autónoma de Mexico, Cuatitlan Izcalli 54740, Mexico
- ⁸ Department of Molecular Biomedicine, Cinvestav Zacatenco, Ciudad de Mexico 07360, Mexico
- * Correspondence: diana.zarate@uanl.edu.mx (D.G.Z.-T.); javier.revilla@comunidad.unam.mx (J.R.R.-V.); mmeraz@cinvestav.mx (M.A.M.-R.); gabriel.luna@cinvestav.mx (G.L.-B.)



Citation: Torres-Ferrer, L.R.; López-Romero, J.M.; Mendez-Nonell, J.; Rivas-Arreola, M.J.; Moreno-Ríos, M.; Ávila-Dávila, E.O.; Prokhorov, E.; Kovalenko, Y.; Zárate-Triviño, D.G.; Revilla-Vazquez, J.R.; et al. Tuning HAuCl_4 /Sodium Citrate Stoichiometry to Fabricate Chitosan-Au Nanocomposites. *Polymers* **2022**, *14*, 788. <https://doi.org/10.3390/polym14040788>

Academic Editor: Maria Gabriella Santonicola

Received: 22 November 2021

Accepted: 28 January 2022

Published: 17 February 2022

Publisher's Note: MDPI stays neutral with regard to jurisdictional claims in published maps and institutional affiliations.



Copyright: © 2022 by the authors. Licensee MDPI, Basel, Switzerland. This article is an open access article distributed under the terms and conditions of the Creative Commons Attribution (CC BY) license (<https://creativecommons.org/licenses/by/4.0/>).

Abstract: Nanocomposite engineering of biosensors, biomaterials, and flexible electronics demand a highly tunable synthesis of precursor materials to achieve enhanced or desired properties. However, this process remains limited due to the need for proper synthesis-property strategies. Herein, we report on the ability to synthesize chitosan-gold nanocomposite thin films (CS/AuNP) with tunable properties by chemically reducing HAuCl_4 in chitosan solutions and different HAuCl_4 /sodium citrate molar relationships. The structure, electrical, and relaxation properties of nanocomposites have been investigated as a function of HAuCl_4 /sodium citrate molar relation. It was shown that gold particle size, conductivity, Vogel temperature (glass transition), and water content strongly depend upon HAuCl_4 /sodium citrate relationships. Two relaxation processes have been observed in nanocomposites; the α -relaxation process, related to a glass transition in wet CS/AuNP films, and the σ -relaxation related to the local diffusion process of ions in a disordered system. The ability to fine-tune both α - and σ -relaxations may be exploited in the proper design of functional materials for biosensors, biomaterials, and flexible electronics applications.

Keywords: chitosan-gold nanocomposites; HAuCl_4 /sodium citrate relationship; α -relaxation; σ -relaxation

1. Introduction

Metal nanoparticles exhibit unique optical, electrical, mechanical, and biomedical properties. In this regard, the number of publications related to polymer-metal nanocomposites has recently increased [1–15]; various studies report on the use of such nanocomposites in biomedicine, biosensors for protein recognition, and flexible electronics. Most of these reports rely on the proper chemical synthesis of Au nanoparticles; however, the challenge to fine-tune the structure, size, and functionality is still at large. In this regard, the synthesis of gold nanoparticles has been studied for more than 20 years to obtain homogenous sizes and

shapes. The preferred method of AuNP synthesis is the well-established Turkevich method, and it is based upon the chemical reduction of HAuCl_4 in a variety of media. AuNPs are then formulated with a variety of polymer matrices used to fabricate nanocomposites for specific applications; the literature reports the best polymer choices for AuNPs are polyvinyl alcohol (PVA), polyvinyl pyrrolidone (PVP), polyethylene glycol (PEO), and the polysaccharide chitosan (CS) [1–16]. Moreover, interesting chemical reduction methods to produce functional metal nanoparticles have been discussed in the literature; in this regard, Ag [17], Au/Ag [18], Pt/Pd [19], and biofunctionalized Au nanoparticles [20]. These studies reveal the importance of proper synthesis methods for biosensor applications.

Based upon the above polymer matrix choices for nanocomposite fabrication, chitosan (CS) has emerged as one of the preferred ones such that it has been extensively studied [21,22]. In this regard, CS is a natural polymer derivative of chitin which is composed of glucosamine and N-acetylglucosamine unit residues; this polysaccharide displays properties such as biocompatibility, biodegradability, and low toxicity [23–26]. The cationic nature of chitosan is primarily responsible for electrostatic interactions with metallic nanoparticles such that it can be used as a stabilizer and reducer of gold forming zero-valent nanoparticles [27–31]. It is noteworthy that the chemical reduction of HAuCl_4 to synthesize AuNPs of specific sizes depends upon the redox agent sodium citrate concentration [29].

Our research group has extensively reported the synthesis of Au NPs by using a modified Turkevich method for a variety of applications [28,30–33]. However, in the literature, there are no reports about the effect of the HAuCl_4 /sodium citrate concentration relationship on the synthesis and final properties of gold nanoparticles using the Turkevich method in chitosan solutions. Chitosan/gold nanoparticle (CS/AuNP) composites find wide application in biomedicine because gold nanoparticles help promote the protein expression in the keratinocytes process regeneration and glioma cells; it has also been shown to be a tool in the detection and treatment of cells cancer [27,29,34]. Moreover, the development of biosensors requires proper optical, piezoelectric, or electrical responses. Electrochemical biosensors, which convert biological binding into useful electrical signals, have received considerable attention in the past years [5,6]. In most cases, AuNPs dispersed in 3D chitosan matrices served as current conductors [5,6,35]. However, the conductivity mechanism of CS/AuNP nanocomposites has not been properly addressed.

This work aims to provide a robust yet simple chemical synthesis route to fabricate CS/AuNPs nanocomposites; these nanocomposites may find potential applications in biosensors, biomaterials, and flexible electronics. In this regard, *in situ* AuNPs are synthesized in chitosan solutions with different HAuCl_4 /sodium citrate relationships. We aim to vary this HAuCl_4 /sodium citrate relationship to tune the structural, electrical, and thermal properties using dielectric spectroscopy, thermogravimetric analysis (TGA), and Fourier transformed infrared spectroscopy (FTIR) measurements.

2. Materials and Methods

2.1. Synthesis of Nanocomposite

Chitosan with medium molecular weight (300,000 g/mol) and 85% of the degree of deacetylation (cat. num. 448877), hydro chloroauric acid (cat. Num. 50790), and sodium citrate (cat. num. S1804) were obtained from Sigma Aldrich® (Lerma, MEX, Mexico) and were used without additional purification.

Seven materials were synthesized with the same molar concentration of HAuCl_4 and different amounts of sodium citrate (SC). The nanocomposites were synthesized by dissolving 2% of chitosan in a 1% acetic acid solution. After that, a 0.3 mM of HAuCl_4 solution was added to different amounts of SC to vary millimolar relationships between HAuCl_4 and SC in the range 0.1 and 5. Then the mixture was heated to 75 °C under magnetic stirring until the solution changed its color to red.

A modified Turkevich chemical reduction method was followed according to a recent study from our group [34]. In this regard, chitosan is a polysaccharide soluble in aqueous acid media below pH 6. At low pH, the amino groups are protonated, allowing the

formation of a water-soluble polyelectrolyte. The amount of citrate added to the reaction should not increase the pH of the solution above 6 to overcome unwanted CS precipitation. Solutions were heated to 75 °C under magnetic stirring until they turned red. Films with a thickness of ca. 20 µm were prepared by the solvent-cast method by pouring the final solution into a plastic Petri dish and allowing the solvent to evaporate for 24 h at 60 °C.

20 µm films were prepared to perform impedance spectroscopy measurements; for FTIR in the transmission mode measurements, ca. 10 µm films were prepared.

2.2. Characterization Studies

2.2.1. Infrared Measurements and Morphology Analysis

The materials were characterized by infrared spectroscopy. FTIR spectra were obtained between 4000 and 400 cm^{-1} (Perkin Elmer Spectrum1 model, PerkinElmer, Inc. Waltham, MA, USA). All spectra were recorded at 4 cm^{-1} intervals and 16 cm^{-1} times scanning using the transmission technique. CS/AuNPs films morphology was imaged by JEOM JSM-7401F field emission scanning electron microscope (JEOL Inc., Peabody, MA, USA). UV-Vis (UV-Vis spectrometer Agilent 8453, Agilent Technologies, Santa Clara, CA, USA) was used to determine the sizes of the gold nanoparticles by the detection of the maximum absorption band in the visible region.

2.2.2. Thermal Measurements

The amount of free water was determined by Thermogravimetric analysis (TGA) (Mettler Toledo 851e model, Mettler Toledo, Columbus, OH, USA). The measurements were performed with a dry airflow from 25 to 300 °C with a rate of 10 °C/min.

2.2.3. Dielectric Measurements

Dielectric measurements in the frequency range from 40 Hz to 110 MHz were carried out with Agilent Precision Impedance Analyzer 4249A (Santa Clara, CA, USA). The amplitude of the measuring signal was 100 mV. Temperature measurements were performed in the cell in the temperature range from 20 °C to 200 °C using a temperature controller programmed to produce a constant heating rate of 3 °C/min between certain measurements temperature. To remove moisture content in the films, additional measurements were carried out in an in-house vacuum cell [36].

3. Results and Discussion

3.1. Infrared Spectroscopy

Figure 1 shows the IR spectra of chitosan-gold nanocomposite with a constant concentration of HAuCl_4 and different amounts of sodium citrate; neat CS, and molar ratios of HAuCl_4 /sodium citrate 0.1, 0.21, 1, 2, and 5. The band at 3300 cm^{-1} is produced by a symmetric stretch of -OH groups. The band at 2880 cm^{-1} is associated with a symmetric stretching of the methyl group, the band present at 1640 cm^{-1} belongs at C=O antisymmetric, from citrate moiety, additionally, the band at 1550 cm^{-1} is assigned to the antisymmetric deformation of NH_3^+ . The band at 1410 cm^{-1} is produced by the C-N stretch. The stretching band at 1025 cm^{-1} is related to C-O [1–3,36].

The salient features of the FTIR spectra are in the vicinity of the 1640 cm^{-1} band, where intensity in the spectrum decreases with decreasing SC concentration. This effect could be attributed to the low efficacy of sodium citrate to reduce gold.

3.2. Morphology Analysis

Figure 2a,b show SEM micrographs where a homogeneous distribution of Au nanoparticles is embedded in the chitosan matrix. Using AutoCAD 2007 software, the dimension of nanoparticles can be assessed. Figure 2c shows particle distribution histogram for HAuCl_4 /SC relation equal to 1; this histogram has been obtained from 3 micrographs. Most nanoparticles are 8 to 11 nm (76%). By increasing the HAuCl_4 /SC from 0 to 1 particle size decreases; upon further increase, particle size slightly increases. Similarly, the maximum

absorption UV-Vis in the ultraviolet-visible spectrum decreases, then it almost remains constant (Figure 2d). The shift of the maximum absorption band to lower wavelength confirms the decrease in AuNP size. In the conventional Turkevich synthesis of AuNPs where sodium citrate is used as a reducing agent (without chitosan), the increasing SC concentration decreases particle size [37]. It is noteworthy that our method, which uses chitosan as a co-reducing agent, helps reduce the amount of sodium citrate, nanoparticle size decreases. This trend can be explained by the reducing capacity of CS and the presence of free amino and hydroxyl groups in chitosan and its polycationic and chelating properties. The special feature of this polysaccharide enables its use as a stabilizer and reducing agent in the synthesis of gold nanoparticles [36]. Additionally, an excess volume of HAuCl_4 promotes the nucleation of smaller particle sizes and polydispersity [36].

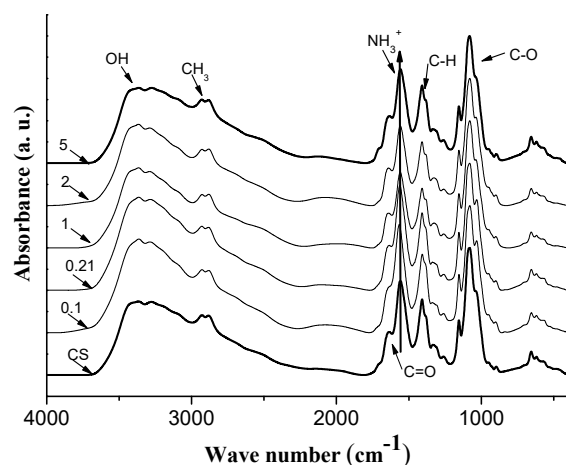


Figure 1. FTIR spectra of neat chitosan (CS) and CS/AuNPs composites with HAuCl_4/SC (M/M, molar ratio) relationships of 0.1, 0.21, 1, 2, and 5. Note the spectral region of ca. 3200 to 3500 cm^{-1} reveals a subtle widening of the vibration bands that are traceable to H-bonding.

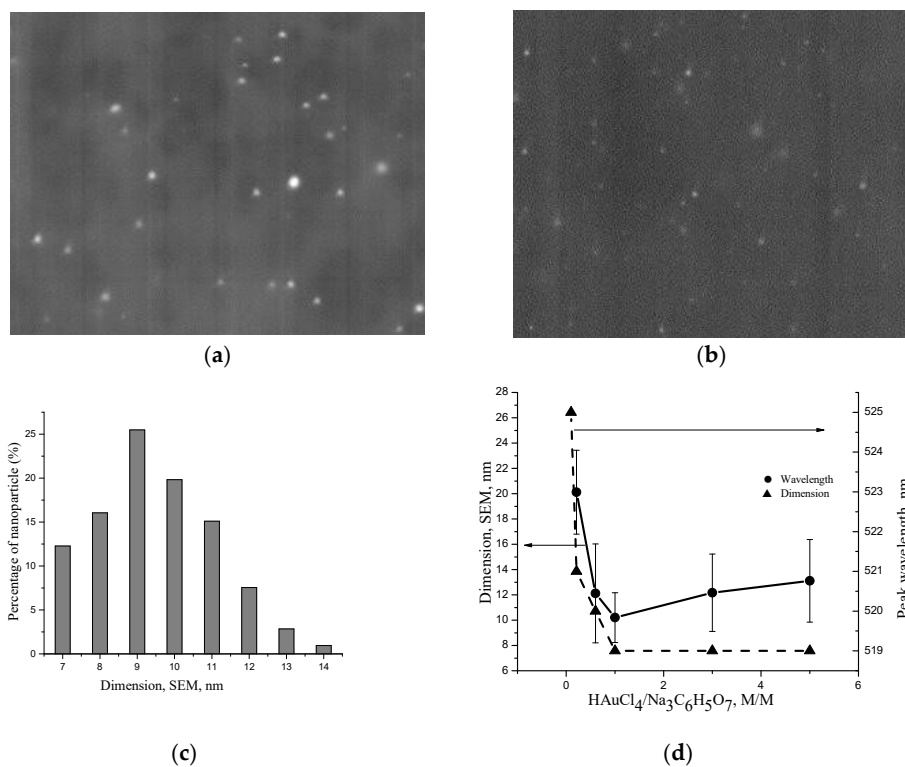


Figure 2. SEM micrographs of CS/AuNPs films with HAuCl_4/SC molar ratios of (a) 0.21 and (b) 1.0. Measurement conditions: Secondary electrons (SE), accelerating voltage 5.0 KV, magnification $\times 100,000$,

working distance (WD) 8.6 mm; (c) Histogram of nanoparticle distribution for HAuCl_4/SC relation equal 1.0; (d) Dependence of maximum absorption in the ultraviolet visible spectrum on HAuCl_4/SC molar ratio.

3.3. Thermal Measurements

Thermogravimetric analysis (TGA) was performed to determine free water content. Free water content may be evaluated by the decrease in sample weight during the heating scan. The weight loss at 120°C is the result of water evaporation. Figure 3 shows the dependence of moisture content as a function of the HAuCl_4/SC molar relationship. Here, an increase in the HAuCl_4/SC molar relationship to 1 and a decrease in moisture content are observed. Upon further increasing this HAuCl_4/SC relationship, free water content slightly decreases, as observed in Figure 3. In this regard, the major change of free water content occurs for HAuCl_4/SC molar relationships from 0 to ca. 1 (ca. 17%), while a minimal change of ca. 3% is observed for up to HAuCl_4/SC molar relationship of 5.

Additional TGA measurements were carried out on films that were annealed for 30 min at 120°C with subsequent cooling to room temperature; a second scan was then performed. In such annealing films, the water content was ca. 0.2 wt.%.

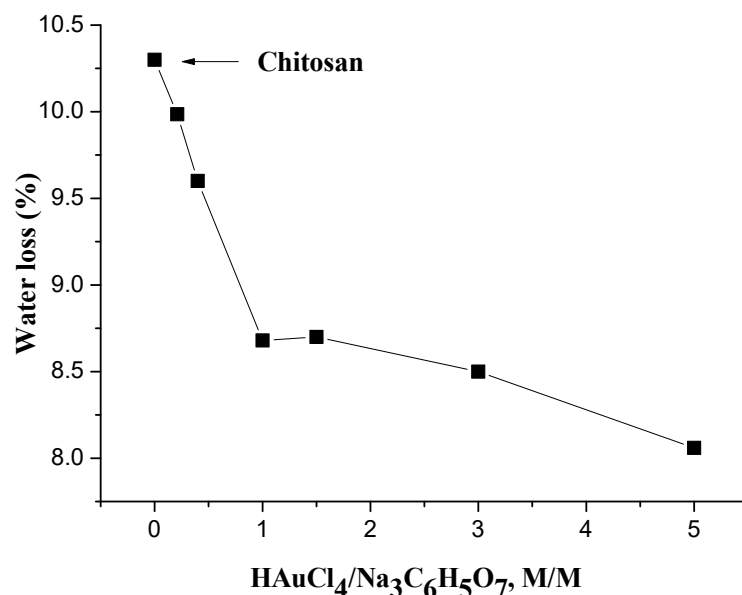


Figure 3. Dependence of water content on HAuCl_4/SC molar relationship.

3.4. Conductivity Measurements

Complex impedance spectra (Z'' versus Z') for all films exhibit characteristic semicircles at high frequencies and a quasi-linear response at low frequencies (insert in Figure 4). The linear response at low frequencies can be associated with interfacial polarization or metal contact effects [27]. The values of DC resistance R_{dc} have been obtained by fitting the high-frequency semicircle of the impedance spectra before interception with real parts of impedance as depicted in the Figure 4 insert. The corresponding DC conductivity (σ_{dc}) has been obtained from the equation $\sigma_{\text{dc}} = d/(R_{\text{dc}} \times S)$, where d is the film thickness and S is the area of film.

From Figure 4, one can observe that the nanocomposite's conductivity increases from 0 up to HAuCl_4/SC molar relationship of ca. 1.0; for higher HAuCl_4/SC molar relationship, the conductivity remains almost constant (saturation). This observation qualitatively agrees with the results shown in Figure 2; there is a saturation of both nanoparticle size and conductivity.

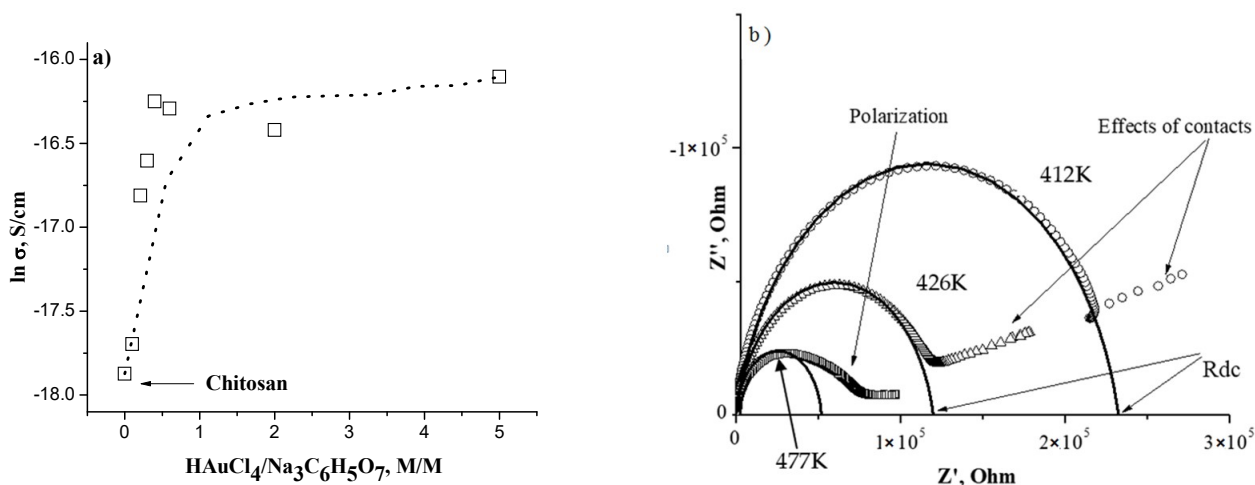


Figure 4. (a) Dependence of DC conductivity on HAuCl₄/SC molar relationship. (b) Insert shows impedance spectra obtained at the temperature indicated on the graph.

3.5. Dielectric Measurements

Dielectric measurements were performed using the Agilent Precision Impedance Analyzer 4249 A in the frequency range from 40 Hz to 110 MHz. The amplitude of the measured signal was 100 mV. Temperatures were measured in the cell from 20 °C to 200 °C using a temperature controller programmed to produce a constant heating rate of 3 °C/min between certain measured temperatures. Each sample was kept for 3 min at each temperature to ensure thermal equilibrium. Additional measurements were conducted in a vacuum cell to remove moisture from the films. As-prepared samples were annealed into the vacuum cell before measurements at 120 °C for 1 h, followed by cooling at room temperature in the vacuum. Additionally, a Peltier heating element was used to perform measurements from 0 °C to 100 °C.

Dielectric measurements can provide information about the temperature relaxation processes in the nanocomposites. In polymer-metal nanoparticle composites, both ionic current and interfacial polarization could often mask the real dielectric relaxation processes in the low-frequency range. Therefore, to analyze the dielectric process, the complex permittivity ϵ^* has been converted to the complex electric modulus M^* by the following equation:

$$M^* = \frac{1}{\epsilon^*} = M' + iM'' = \frac{\epsilon'}{\epsilon'^2 + \epsilon''^2} + i \frac{\epsilon''}{\epsilon'^2 + \epsilon''^2} \quad (1)$$

where M' is the real and M'' the imaginary part of electric modulus, ϵ' is the real and ϵ'' the imaginary part of permittivity. In this representation, interfacial polarization and electrode contributions are essentially suppressed [27]. The corresponding relaxation time can be calculated by the next relation: $\tau = 1/(2\pi f_p)$, where f_p is the peak frequency in the dependence of M'' on frequency [38].

It is noteworthy that a recent study of our group reported three molecular relaxations in CS-Au nanocomposites based upon dielectric measurements [38]:

- (1) in the temperature range of 25–70 °C, a nonlinear behavior is revealed,
- (2) a linear behavior in the temperature range of 70–150 °C, and
- (3) at temperatures above 160 °C, polymer degradation is triggered.
- (4) Based upon this analysis, Figure 5 shows the dependencies of the relaxation time on reciprocal temperature based upon the methodology described in [27] for a HAuCl₄/SC molar relationship of 0.21.

In the temperature range of 25–70 °C the nonlinear relaxation process can be fitted by the Vogel–Fulcher–Tammann (VFT) relationship $\tau = \tau_0 \exp(\frac{D}{T-T_0})$, where T_0 is Vogel temperature, τ_0 and D are empirical material-dependent parameters.

In the linear relaxation process (80–150 °C), an Arrhenius-type linear dependency was observed ($\tau = \tau_0 \exp(\frac{E_{act}}{RT})$) for as-prepared films and in the temperature range 22–150 °C for dry films (annealed in vacuum to the temperature of 120 °C).

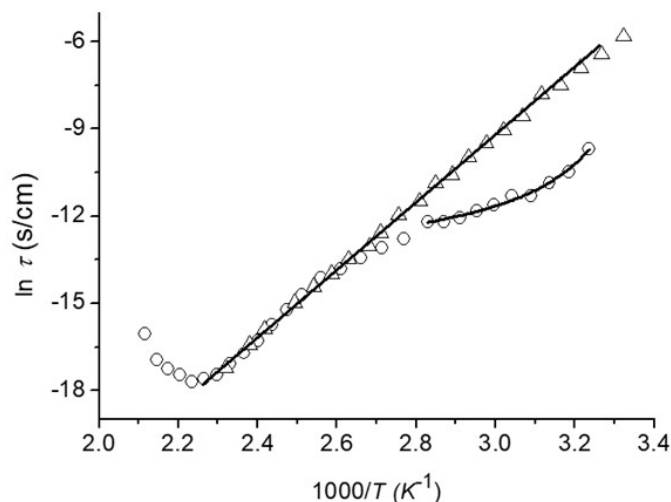


Figure 5. Dependence of the relaxation time on the reciprocal temperature in as-prepared (open circles) and annealed films (open triangles) for H_{AuCl₄}/SC molar relationship of 0.21. Note an Arrhenius-type linear fit associated with σ -relaxation (activation energy ca. 103.2 kJ/mol) and the nonlinear VFT fit associated with an α -relaxation (glass transition).

The σ -relaxation appears when there is dominance of ionic conductivity in CS-Au nanocomposites and in neat chitosan and most polysaccharides [36]. This relaxation appears due to ion migration which is responsible for additional dielectric polarization in amorphous and electrically inhomogeneous systems.

The nonlinear α -relaxation, which is related to a glass transition, appears in wet CS-Au nanocomposites. Figure 6 shows the Vogel temperature T_0 as a function of the H_{AuCl₄}/SC molar relationship; an analogous behavior for the glass transition temperature of such nanocomposites is expected at 50–70 K higher than T_0 [38].

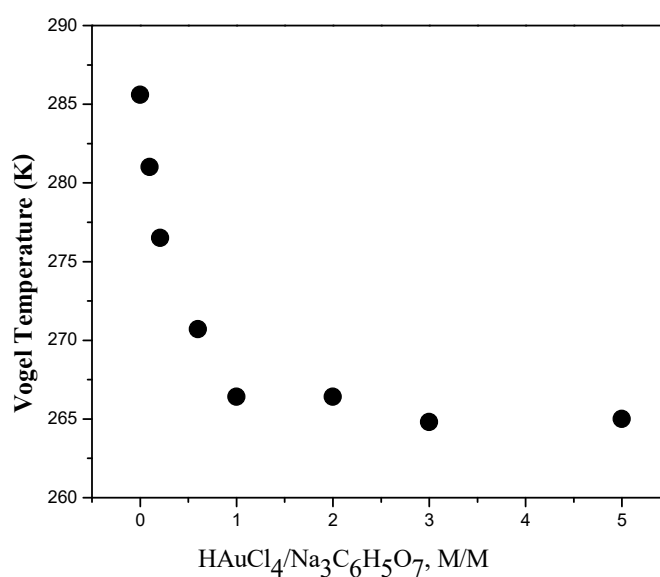


Figure 6. Dependence of Vogel temperature on H_{AuCl₄}/SC molar relationship. Note that for most amorphous polymers, the glass transition is 50–70 K higher than T_0 .

Figure 6 shows the existence of excess HAuCl_4 is responsible for the “anomaly” dependence of Vogel temperature. The Vogel temperature T_0 is the apparent activation temperature of the α -relaxation in many polymers; T_0 is usually 50–70 K lower than glass transition temperature [34].

4. Discussion

In this work, CS/Au nanocomposites have been prepared with different HAuCl_4/SC molar relationships; this means that some HAuCl_4 will be complexed in the films and can participate in the observed ionic DC conductivity. By decreasing the concentration of SC (an increase in HAuCl_4), there is an increase in the film’s conductivity. When the HAuCl_4/SC molar relationship is higher than 1.0, a competitive reducing capacity of chitosan helps compensate for the reduced amount of SC. The ability of chitosan to help reduce HAuCl_4 is due to the presence of free amino and hydroxyl groups. This effect is responsible for saturation in the particle size (Figure 2c), conductivity (Figure 4), water absorption (Figure 3), and Vogel temperature (Figure 6).

The presence of water absorption in neat chitosan films promotes a plasticizing effect; for this reason, in the samples with lower moisture content, the Vogel temperature is lowered [38]. Nevertheless, in the case of CS/AuNP nanocomposites, the Vogel temperature decreases with increasing HAuCl_4/SC molar relationship even though moisture content decreases (see Figures 3 and 6). According to our previous work [36], gold nanoparticles at low HAuCl_4/SC molar relationship attach to chitosan through hydrogen bonds between complexed sodium and the amino groups of chitosan. Upon increasing the HAuCl_4/SC molar relationship, complexed sodium decreases, and the interaction between AuNPs and chitosan could be due to electrostatic forces (due to the polarization of nanoparticle surface. This effect is responsible for the decreasing of Vogel and glass transition temperatures. A similar conclusion can be drawn from the dependencies of particle size (Figure 2c) and the conductivity at HAuCl_4/SC molar relationships higher than 1.0.

It is noteworthy that by varying the HAuCl_4/SC molar relationship, the nanocomposite’s water absorption, conductivity, and the glass transition temperature can be fine-tuned. Samples prepared with low HAuCl_4/SC molar relationships have higher complexed sodium molecules. These molecules form hydrogen bonds with the polymer matrix, and water can attach to the OH group of chitosan. On the other hand, the films with high HAuCl_4/SC molar relationships have less complex sodium molecules such that the quantity of hydrogen bonds is also lower. Additionally, any excess of HAuCl_4 can potentially be reduced by the chitosan’s reducing capabilities. Although the reducing process by chitosan is not well understood, it is possible that the OH groups can act as reducing groups in the formation of nanoparticles [39]. Au nanoparticles that are charged superficially can attach to NH_3^+ groups by electrostatic forces. The nanocomposite water absorption is lower for materials with higher HAuCl_4/SC molar relationships due to the decreasing hydrogen bonding capacity.

5. Conclusions

CS/AuNP thin films have been synthesized by chemical reduction of HAuCl_4 in the presence of sodium citrate (SC) and chitosan solutions. The structure, conductivity, and relaxation properties of CS/AuNPs films have been investigated as a function of the HAuCl_4/SC molar relationship. Our results show that HAuCl_4/SC molar relationship affects the AuNP sizes because of the additional chitosan reducing agent capabilities. A descriptive model for understanding the reaction between HAuCl_4 , sodium citrate chitosan, and acetic acid has been proposed. We have shown that an excess of HAuCl_4 is responsible for dependencies of conductivity, Vogel temperature, and water absorption in CS/AuNPs nanocomposites. The value of HAuCl_4/SC molar relationship of ca. 1.0 is a molar relationship threshold. At higher HAuCl_4/SC molar relationships, the reducing capacity of chitosan leads to saturation of free HAuCl_4 amount and subsequently to saturation in all properties of CS/AuNP nanocomposites.

Author Contributions: Conceptualization, G.L.-B., M.A.M.-R., D.G.Z.-T., J.R.R.-V.; methodology, L.R.T.-F., J.M.L.-R., M.J.R.-A., J.M.-N.; software, Y.K., E.P.; validation, E.O.Á.-D., M.M.-R.; formal analysis, E.O.Á.-D., M.M.-R.; investigation, L.R.T.-F., G.L.-B., M.A.M.-R., D.G.Z.-T., J.R.R.-V.; resources, J.M.L.-R., M.J.R.-A., J.M.-N.; data curation, Y.K., E.P.; writing—original draft preparation, L.R.T.-F., G.L.-B., D.G.Z.-T.; writing—review and editing, L.R.T.-F., G.L.-B.; visualization, G.L.-B., M.A.M.-R.; supervision, G.L.-B., M.A.M.-R.; project administration, G.L.-B., M.A.M.-R.; funding acquisition, G.L.-B., M.A.M.-R., D.G.Z.-T., J.R.R.-V. All authors have read and agreed to the published version of the manuscript.

Funding: This research was funded by Consejo Nacional de Ciencia y Tecnología (CONACYT) under internal project 286926 and by Dirección Cinvestav-Querétaro.

Institutional Review Board Statement: Not applicable.

Informed Consent Statement: Not applicable.

Data Availability Statement: The data presented in this study are available on request from the corresponding author.

Acknowledgments: This work was partially supported by CONACYT, Mexico. The authors are grateful to J.A. Muñoz-Salas for technical assistance in electrical measurements and Araceli Mauricio-Sanchez for FTIR measurements.

Conflicts of Interest: The authors declare no conflict of interest.

References

1. Bhumkar, D.R.; Joshi, H.M.; Sastry, M.; Pokharkar, V.B. Chitosan reduced gold nanoparticles as novel carriers for transmucosal delivery of insulin. *Pharm. Res.* **2007**, *24*, 1415–1426. [[CrossRef](#)]
2. Esther, J.; Sridevi, V. Synthesis and characterization of chitosan-stabilized gold nanoparticles through a facile and green approach. *Gold Bull.* **2017**, *50*, 1–5. [[CrossRef](#)]
3. Jeyarani, S.; Vinita, N.M.; Puja, P.; Senthamilselvi, S.; Devan, U.; Velangani, A.J.; Biruntha, A.; Pugazhendhi, P.; Kumar, J. Biomimetic gold nanoparticles for its cytotoxicity and biocompatibility evidenced by fluorescence-based assays in cancer (MDA-MB-231) and non-cancerous (HEK-293) cells. *Photochem. Photobiol. B* **2020**, *202*, 111715. [[CrossRef](#)]
4. Da Silva, A.B.; Rufato, K.B.; de Oliveira, A.C.; Souza, P.R.; da Silva, E.P.; Muniz, E.C.; Vilsinski, B.H.; Martins, A.F. Composite materials based on chitosan/gold nanoparticles: From synthesis to biomedical applications. *Int. J. Biol. Macromol.* **2020**, *161*, 977–998. [[CrossRef](#)]
5. Hu, L.; Fu, X.; Kong, G.; Yin, Y.; Meng, H.M.; Ke, G.; Zhang, X.B. DNAzyme-gold nanoparticle-based probes for biosensing and bioimaging. *J. Mater. Chem. B* **2020**, *8*, 9449–9465. [[CrossRef](#)]
6. Falahati, M.; Attar, F.; Sharifi, M.; Saboury, A.A.; Salihi, A.; Aziz, F.M.; Kostova, I.; Burda, C.; Priecl, P.; Lopez-Sanchez, J.A.; et al. Gold nanomaterials as key suppliers in biological and chemical sensing, catalysis, and medicine. *Biochim. Biophys. Acta BBA Gen. Subj.* **2020**, *1864*, 129435. [[CrossRef](#)]
7. Xu, Q.; Mao, C.; Liu, N.N.; Zhu, J.J.; Sheng, J. Direct electrochemistry of horseradish peroxidase based on biocompatible carboxymethyl chitosan-gold nanoparticle nanocomposite. *Biosens. Bioelectron.* **2006**, *22*, 768–773. [[CrossRef](#)]
8. Zeng, J.; Gong, M.; Wang, D.; Li, M.; Xu, W.; Li, Z.; Yin, Y. Direct Synthesis of Water-Dispersible Magnetic/Plasmonic Hetero-nanostructures for Multimodality Biomedical Imaging. *Nano Lett.* **2019**, *19*, 3011–3018. [[CrossRef](#)]
9. Wei, D.H.; Lin, T.K.; Liang, Y.C.; Chang, H.W. Formation and Application of Core-Shell of FePt-Au Magnetic-Plasmonic Nanoparticles. *Front. Chem.* **2021**, *9*, 181. [[CrossRef](#)]
10. Vidotti, M.; Carvalhal, R.F.; Mendes, R.K.; Ferreira, D.C.M.; Kubot, L.T. Biosensors based on gold nanostructures. *J. Braz. Chem. Soc.* **2011**, *22*, 3–20. [[CrossRef](#)]
11. Liu, Y.; Yuan, R.; Chai, Y.; Hong, C.; Guan, S. Preparation of a composite film electrochemically deposited with chitosan and gold nanoparticles for the determination of α -1-fetoprotein. *Bioprocess Biosyst. Eng.* **2010**, *33*, 613–618. [[CrossRef](#)]
12. Haiyan, J.; Taotao, Y.; Yinxiu, Z.; Wenmin, W.; Jingkun, X.; Limin, L.; Ping, L. Immunosensor for α -fetoprotein based on a glassy carbon electrode modified with electrochemically deposited N-doped graphene, gold nanoparticles and chitosan. *Microchim. Acta* **2017**, *184*, 3747–3753.
13. Xue, M.H.; Xu, Q.; Zhou, M.; Zhu, J.J. In situ immobilization of glucose oxidase in chitosan-gold nanoparticle hybrid film on Prussian Blue modified electrode for high-sensitivity glucose detection. *Electrochem. Commun.* **2006**, *8*, 1468–1474. [[CrossRef](#)]
14. Shan, C.; Yang, H.; Han, D.; Zhang, Q.; Ivaska, A.; Niu, L. Graphene/AuNPs/chitosan nanocomposites film for glucose biosensing. *Biosens. Bioelectron.* **2010**, *25*, 1070–1074. [[CrossRef](#)]
15. Rassas, I.; Braiek, M.; Bonhomme, A.; Bessueille, F.; Raffin, G.; Majdoub, H.; Jaffrezic-Renault, N. Highly sensitive voltammetric glucose biosensor based on glucose oxidase encapsulated in a chitosan/kappa-carrageenan/gold nanoparticle bionanocomposite. *Sensors* **2019**, *19*, 154. [[CrossRef](#)]

16. Kimling, J.; Maier, M.; Okenve, B.; Kotaidis, V.; Ballot, H.; Plech, A. Turkevich Method for Gold Nanoparticle Synthesis Revisited. *J. Phys. Chem. B* **2006**, *110*, 15700–15707. [[CrossRef](#)]
17. Xavier, S.S.J.; Karthikeyan, C.; Kumar, G.G.; Kim, A.R.; Yoo, D.J. Colorimetric detection of melamine using β -cyclodextrin-functionalized silver nanoparticles. *Anal. Methods* **2014**, *6*, 8165–8172. [[CrossRef](#)]
18. Kim, W.-J.; Kim, S.; Kim, A.R.; Yoo, D.J. Direct Detection System for Escherichia coli Using Au–Ag Alloy Microchips. *Ind. Eng. Chem. Res.* **2013**, *52*, 7282–7288. [[CrossRef](#)]
19. Kumar, T.R.; Yoo, D.J.; Kim, A.R.; Kumar, G.G. Green synthesis of Pt–Pd bimetallic nanoparticle decorated reduced graphene oxide and its robust catalytic activity for efficient ethylene glycol electrooxidation. *New J. Chem.* **2018**, *42*, 14386–14393. [[CrossRef](#)]
20. Kim, W.-J.; Choi, S.-H.; Rho, Y.-S.; Yoo, D.J. Bio-functionalized Gold Nanoparticles for Surface-Plasmon-Absorption-Based Protein Detection. *Bull. Korean Chem. Soc.* **2011**, *32*, 4171–4175. [[CrossRef](#)]
21. Virgili, A.H.; Laranja, D.C.; Malheiros, P.S.; Pereira, M.B.; Costa, T.M.; de Menezes, E.W. Nanocomposite film with antimicrobial activity based on gold nanoparticles, chitosan and aminopropylsilane. *Surf. Coat. Technol.* **2021**, *415*, 127086. [[CrossRef](#)]
22. Regiel-Futyra, A.; Kus-Liskiewicz, M.; Sebastian, V.; Irusta, S.; Arruebo, M.; Stochel, G.; Kyziol, A. Development of Noncytotoxic Chitosan–Gold Nanocomposites as Efficient Antibacterial Materials. *ACS Appl. Mater. Interfaces* **2015**, *7*, 1087–1099. [[CrossRef](#)]
23. Tao, F.; Cheng, Y.; Shi, X.; Zheng, H.; Du, Y.; Xiang, W.; Deng, H. Applications of chitin and chitosan nanofibers in bone regenerative engineering. *Carbohydr. Polym.* **2020**, *230*, 115658. [[CrossRef](#)]
24. Sun, I.C.; Na, J.H.; Jeong, S.Y.; Kim, D.E.; Kwon, I.C.; Choi, K.; Ahn, C.H.; Kim, K. Biocompatible glycol chitosan-coated gold nanoparticles for tumor-targeting CT imaging. *Pharm. Res.* **2014**, *31*, 1418–1425. [[CrossRef](#)]
25. Collado-González, M.; Espín, V.F.; Montalbán, M.G.; Pamies, R.; Cifre, J.G.H.; Baños, F.G.D.; Villora, G.; de la Torre, J.G. Aggregation behaviour of gold nanoparticles in presence of chitosan. *J. Nanopart. Res.* **2015**, *17*, 268. [[CrossRef](#)]
26. Katas, H.; Lim, C.S.; Azlan, A.Y.H.N.; Buang, F.; Busra, M.F.M. Antibacterial activity of biosynthesized gold nanoparticles using biomolecules from *Lignosus rhinocerotis* and chitosan. *Saudi Pharm. J.* **2019**, *27*, 283–292. [[CrossRef](#)]
27. Choi, M.; Cho, M.; Han, B.; Hong, J.; Jeong, J.; Park, S.; Cho, M.; Kim, K.; Cho, W. Chitosan nanoparticles show rapid extrapulmonary tissue distribution and excretion with mild pulmonary inflammation to mice. *Toxicol. Lett.* **2010**, *199*, 144–152. [[CrossRef](#)]
28. Valenzuela-Acosta, E.M.; Prokhorov, E.; de Fuentes, O.A.; Luna-Barcenas, G.; Mauricio-Sánchez, R.A.; Elizalde-Pena, E.A. Chitosan-Gold Nanocomposite for Copper Ions Detection. *Curr. Nanosci.* **2016**, *12*, 754–761. [[CrossRef](#)]
29. Shuangyun, L.; Donglin, X.; Guijuan, H.; Hongxia, J.; Yufei, W.; Haiying, G. Concentration effect of gold nanoparticles on proliferation of keratinocytes. *Colloids Surf. B* **2010**, *81*, 406–411.
30. Vergara-Castañeda, H.; Granados-Segura, L.O.; Luna-Bárceñas, G.; McClements, D.J.; Herrera-Hernández, M.G.; Arjona, N.; Hernández-Martínez, A.R.; Estevez, M.; Pool, H. Gold nanoparticles bio-reduced by natural extracts of arantho (*Kalanchoe daigremontiana*) for biological purposes: Physico-chemical, antioxidant and antiproliferative evaluations. *Mater. Res. Express* **2019**, *6*, 055010. [[CrossRef](#)]
31. Velazquez-Hernandez, I.; Estevez, M.; Vergara-Castañeda, H.; Guerra-Balcazar, M.; Alvarez-Contreras, L.; Luna-Barcenas, G.; Perez, C.; Arjona, N.; Pool, H. Synthesis and application of biogenic gold nanomaterials with {1 0 0} facets for crude glycerol electro-oxidation. *Fuel* **2020**, *279*, 118505. [[CrossRef](#)]
32. Kumar, K.S.; Kumar, G.; Prokhorova, E.; Luna-Bárceñas, G.; Buitronb, G.; Khannac, V.G.; Sanchez, I.C. Exploitation of anaerobic enriched mixed bacteria (AEMB) for the silver and gold nanoparticles synthesis. *Colloids Surf. A Physicochem. Eng. Aspects* **2014**, *462*, 264–270. [[CrossRef](#)]
33. Mendoza, M.O.; Valenzuela-Acosta, E.M.; Prokhorov, E.; Luna-Barcenas, G.; Kumar-Krishnan, S. Percolation Phenomena in Polymer Nanocomposites. *Adv. Mater. Lett.* **2016**, *7*, 353–359. [[CrossRef](#)]
34. Jing, L.; Lei, W.; Xiang, Y.; Zhi, P.; Hong, C. In vitro cancer cell imaging and therapy using transferrin-conjugated gold nanoparticles. *Cancer Lett.* **2009**, *274*, 319–326.
35. Ding, L.; Hao, C.; Xue, Y.; Ju, H. A bio-inspired support of gold nanoparticles-chitosan nanocomposites gel for immobilization and electrochemical study of K562 leukemia cells. *Biomacromolecules* **2007**, *8*, 1341. [[CrossRef](#)]
36. Strupiechonski, E.; Moreno-Ríos, M.; Ávila-Dávila, E.O.; Román-Doval, R.; Prokhorov, E.; Kovalenko, Y.; Zárate-Triviño, D.G.; Medina, D.I.; Luna-Barcenas, G. Relaxation Phenomena in Chitosan-Au Nanoparticle Thin Films. *Polymers* **2021**, *13*, 3214. [[CrossRef](#)]
37. Turkevich, J.; Stevenson, P.C.; Hiller, J.J.R. A Study of the nucleation and growth processes in the synthesis of colloidal gold. *Discuss. Faraday Soc.* **1951**, *11*, 55–75. [[CrossRef](#)]
38. González-Campos, J.B.; Prokhorov, E.; Luna-Bárceñas, G.; Fonseca-García, A.; Sanchez, I.C.J. Dielectric relaxations of chitosan: The effect of water on the α -relaxation and the glass transition temperature. *Polym. Sci. Part B Polym. Phys.* **2009**, *47*, 2259–2271. [[CrossRef](#)]
39. Prokhorov, E.; Luna-Barcenas, G.; Kumar-Krishnan, S.; Sánchez, R.A.M.; Reyes, B.E.C.; Vargas, J.H. Probing molecular interactions of polysaccharides in the presence of water. *J. Mol. Struct.* **2020**, *1218*, 128531. [[CrossRef](#)]